Multinucleon transfer processes in ^{40}Ca+^{208}Pb

S. Szilner,[1,5] L. Corradi,[1] G. Pollarolo,[2] S. Beghini,[3] B. R. Behera,[1] E. Fioretto,[1] A. Gadea,[1] F. Haas,[4] A. Latina,[1] G. Montagnoli,[3] F. Scarlassara,[3] A. M. Stefanini,[1] M. Trotta,[1,*] A. M. Vinodkumar,[1] and Y. Wu[1]

[1]*Istituto Nazionale di Fisica Nucleare, Laboratori Nazionali di Legnaro, I-35020 Legnaro, Italy*

[2]*Dipartimento di Fisica Teorica, Università di Torino, and Istituto Nazionale di Fisica Nucleare, I-10125 Torino, Italy*

[3]*Dipartimento di Fisica, Università di Padova, and Istituto Nazionale di Fisica Nucleare, I-35131 Padova, Italy*

[4]*Institut de Recherches Subatomiques, CNRS-IN2P3/ULP et Université Louis Pasteur, F-67037 Strasbourg, France*

[5]*Ruđer Bosković Institute, HR-10 002 Zagreb, Croatia*

(Received 30 December 2004; published 28 April 2005)

Multinucleon transfer reactions in ^{40}Ca+^{208}Pb have been studied at bombarding energies close to the Coulomb barrier. Projectilelike fragments have been identified in nuclear mass and charge with a time-of-flight spectrometer. Angular and total kinetic energy loss distributions and inclusive cross sections have been compared with those of semiclassical models. The analysis shows that a successive transfer mechanism of single nucleons does not account for the data, and a direct nucleon pair transfer has to be included in the description. Nucleon evaporation effects are taken into account.

DOI: 10.1103/PhysRevC.71.044610 PACS number(s): 25.70.Hi, 24.10.−i, 25.70.Bc

I. INTRODUCTION

Nuclear reactions where few quanta—energy, angular momentum, and number of nucleons—are exchanged between projectile and target, provide an important tool to study the properties of nuclei close to their ground states. Among the different kinds of quasielastic reactions, the exchange of nucleons is peculiar because such reactions provide specific information on single-particle levels and correlations. The extensive experimental work with light-ion reactions, for example, gave considerable inputs to the pairing model. With heavy ions, these studies can be further extended. The two colliding partners can exchange a large number of nucleons, thus enabling to probe the pair density in the nuclear medium, that is, to probe the ability of two nucleons to form pairs of zero angular momentum [1]. From the reaction mechanism point of view, the study of multinucleon transfer reactions provides an insight about which degrees of freedom have to be included in any model to describe the evolution of the heavy-ion reaction from the quasielastic to the deep inelastic regimes and to fusion.

Extensive work on multinucleon transfer have been carried out during past years [2,3]. These studies allowed to extract the radial dependence of the average transfer form factors for the different channels. Enhancement factors have been introduced to explain the deviation from the naive picture that in an uncorrelated medium the probability for the transfer of two nucleons is simply given by the product of the probability for the transfer of a single nucleon. In recent studies [4,5] a complete identification of the final reaction products has been achieved up to six neutron and proton transfer channels. The comparison between data and calculations, based on semiclassical models [6–9], allowed to identify the different degrees of freedom that influence the evolution of the reaction, such as deformation, single, and pair transfer modes.

Closed-shell nuclei constitute an almost ideal case for a quantitative comparison with calculations. Therefore, we have studied multinucleon transfer processes for the system ^{40}Ca+^{208}Pb at energies close to the Coulomb barrier. The differential and total cross sections and the total kinetic energy loss are reported and compared with semiclassical models. The results of pure neutron transfer channels were presented in a recent publication [10]. In this article we discuss the results for all multinucleon transfer channels.

II. EXPERIMENT AND EXPERIMENTAL RESULTS

The experiment was performed using the Tandem+ALPI accelerator complex of the Laboratori Nazionali di Legnaro. A ^{40}Ca beam was accelerated onto a ^{208}Pb target (200 μg/cm^2, sandwiched between carbon foils) at incident energies of 235 and 249 MeV, which correspond to 5 and 15%, respectively above the nominal Coulomb barrier. Projectilelike fragments were detected with the time-of-flight spectrometer PISOLO [11], which combines a large solid angle ($\simeq 3$ msr) and a good mass and a charge resolution ($\Delta A/A \simeq 1/100$ and $\Delta Z/Z \simeq 1/60$). Time-of-flight signals were derived from two microchannel plate detectors, whereas a multianode transverse field ionization chamber was used for nuclear charge and energy determination [5,11]. Absolute normalization of the cross sections was ensured by four silicon monitors detecting elastically scattered ^{40}Ca ions. To cover most of the transfer flux the measurements have been performed in the angular range $42^\circ < \theta_{\rm lab} < 115^\circ$ for the lower energy ($E_{\rm lab} = 235$ MeV) and $42^\circ < \theta_{\rm lab} < 100^\circ$ for the higher bombarding energy ($E_{\rm lab} = 249$ MeV).

Examples of A-Z and E-ΔE two-dimensional spectra obtained at $E_{\rm lab} = 235$ MeV at the grazing angle are displayed in Fig. 1. A clear identification of the nuclear charge and mass of projectilelike fragments is obtained. In the right panel, the dashed lines correspond to the pure neutron pickup (ΔN) and the pure proton stripping (ΔZ) and the full line represents the

*Present address: INFN-Sezione di Napoli, 1-80126, Napoli, Italy.

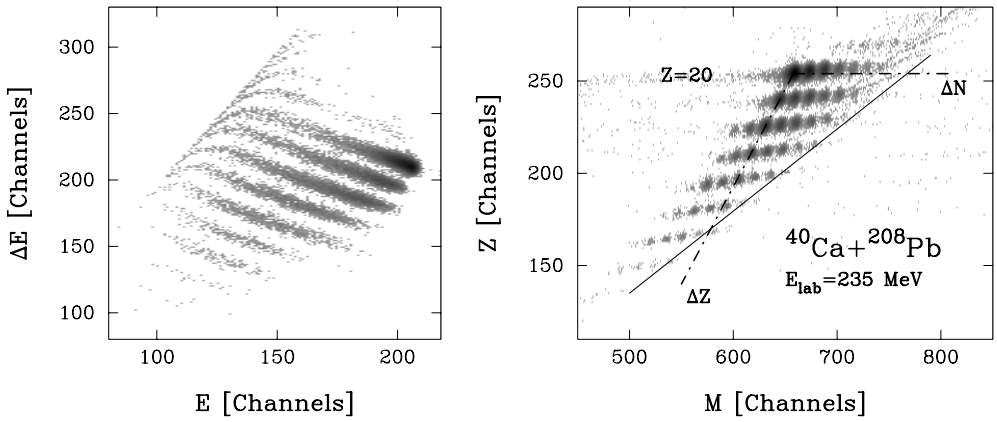

FIG. 1. E-ΔE two-dimensional spectra (left panel) and mass-charge distribution (right panel) of the ^{40}Ca+^{208}Pb reaction at $E_{\rm lab} =$ 235 MeV obtained at the grazing angle, $\theta_{\rm lab} = 84^{\circ}$. The dash-dotted lines correspond to the pure proton stripping (ΔZ) and to the pure neutron pickup (ΔN) channels, crossing at $Z = 20$ and $A = 40$. The full line shows the charge equilibrization, namely the N/Z ratio of the compound nucleus.

charge equilibrization, namely the location of the N/Z ratio of the compound nucleus. We observe that the final nuclei are all to the left side of this line, indicating the dominance of a direct mechanism where the nucleon transfer follows the path expected from optimum Q-value arguments that favor the neutron pickup and the proton stripping. We also notice that for massive proton transfer channels, the isotopic distribution drifts toward lower masses.

The total cross sections, obtained from integrating the angular and Q-value distributions for each isotope, are shown in Fig. 2 for pure proton stripping and pure neutron pickup channels. The cross sections for the neutron pickup drop by almost a constant factor for each transferred neutron, as an independent particle mechanism would suggest. The pure proton cross sections behave differently, with the population of the $-2p$ channel as strong as the $-1p$. This suggests the contribution of processes involving the transfer of proton pairs in addition to the successive transfer of single protons.

As mentioned above, for massive proton transfer ($\Delta Z > 3$) the yield drifts toward lower masses (see Fig. 1), indicating that evaporation processes influence the final isotopic distributions. This can be seen directly from the data by plotting them as a function of the transferred protons (ΔZ) for each neutron channel, as shown in Fig. 3 for the two bombarding energies. The left panels group the data associated with neutron pickup, whereas the middle panels group those involving neutron stripping. The regular pattern of the left panel is compatible with a successive mechanism where neutrons and protons act independently. The irregular behavior seen in the middle panels indicates that the same picture cannot be drawn for channels involving neutron stripping. The fact that neutrons and protons are transferred independently is also stressed from the pattern in the right panels where the data are plotted as a function of the neutron transfer (ΔN) for each nuclear charge.

The total kinetic energy loss (TKEL) distributions derived by assuming a pure binary process are shown in Figs. 4 and 5 for selected channels. The TKEL corresponding to the two touching spheres configuration for each channel are shown

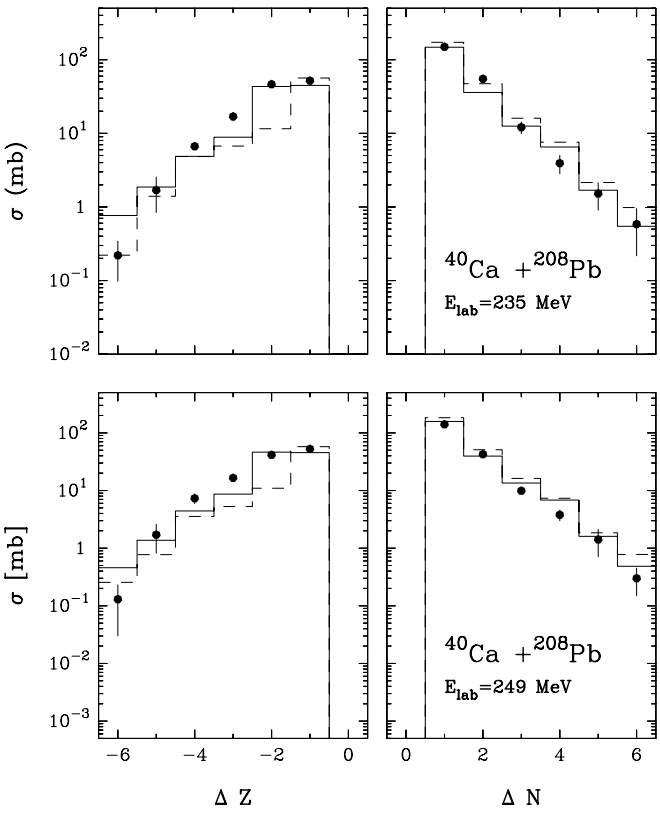

FIG. 2. Angle and Q-value integrated cross sections for pure proton stripping and pure neutron pickup channels of the ^{40}Ca+^{208}Pb reaction at $E_{\rm lab} = 235$ (top) and 249 (bottom) MeV as a function of transferred nucleons. The points and histograms are experimental and theoretical (CWKB) values, respectively. The dashed lines are the results of CWKB calculations using sequential transfer only, whereas the solid lines also include pair-transfer modes.

as vertical lines to indicate the maximal amount of energy that can be lost in a binary collision. Events with larger energy losses correspond to binary events with large deformation. The data are between two limiting situations, one corresponding to

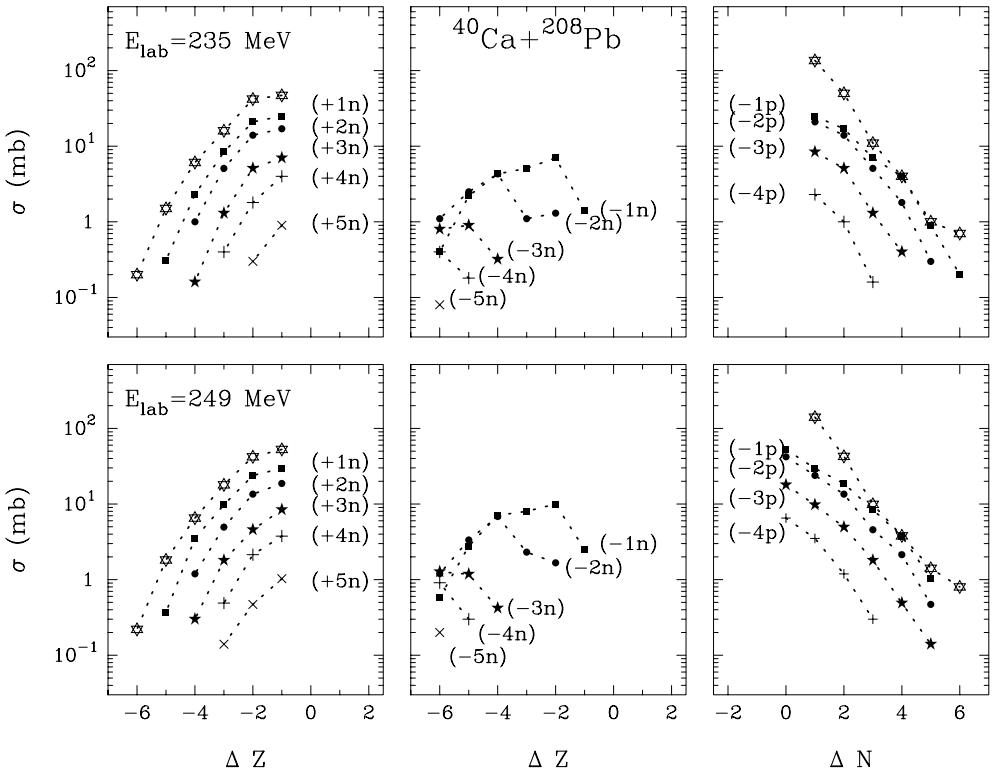

FIG. 3. Angle and energy integrated cross sections at 235 (upper panel) and 249 (lower panel) MeV. The left and middle panels show total cross sections as a function of transferred protons for neutron pickup and neutron stripping reactions, respectively. The right panels show the total cross sections as a function of the number of transferred neutrons. For the sake of clarity, no experimental errors are plotted.

direct reactions with narrow distributions close to the ground to ground state Q value and another with distributions centered at the touching sphere configuration corresponding to fully relaxed events. Large energy losses are more pronounced as more nucleons are transferred and moving toward forward angles.

The angular distributions obtained by integrating the full TKEL range for the bombarding energies of 235 and 249 MeV are shown in Fig. 6. The figure also depicts the quasielastic angular distributions for ^{40}Ca events that allow to extract the optical potential and thus to estimate the total reaction cross sections. For the indicated channels, the angular distributions are bell shaped with a forward tail that becomes more pronounced when more nucleons are transferred. Such behavior [12] indicates that this angular region receives contribution from deep inelastic processes (see also Fig. 5,

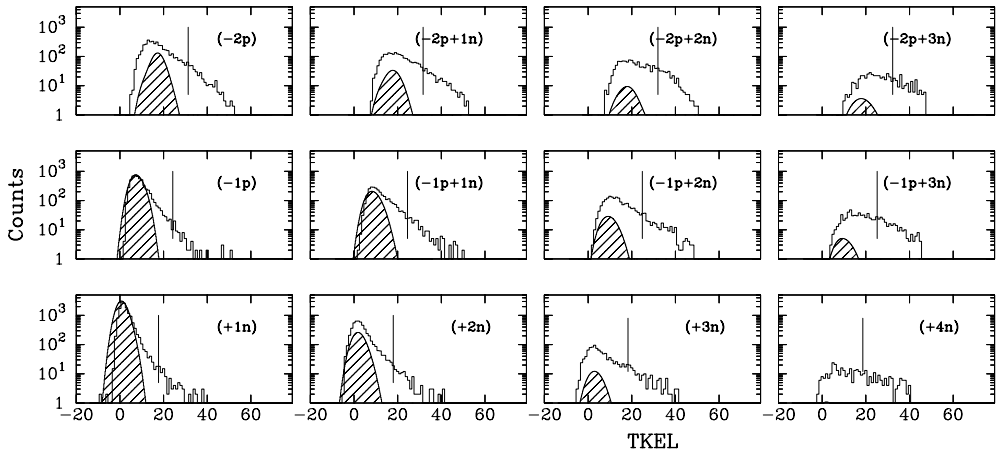

FIG. 4. Experimental (histogram) and theoretical (shaded areas) total kinetic energy loss distributions at $\theta_{lab} = 84^\circ$ at $E_{lab} = 235$ MeV for the strongest transfer channels. Vertical lines indicate the total kinetic energy loss corresponding to the two-touching-sphere configuration of the appropriate Z_1 and Z_2 in the exit channels.

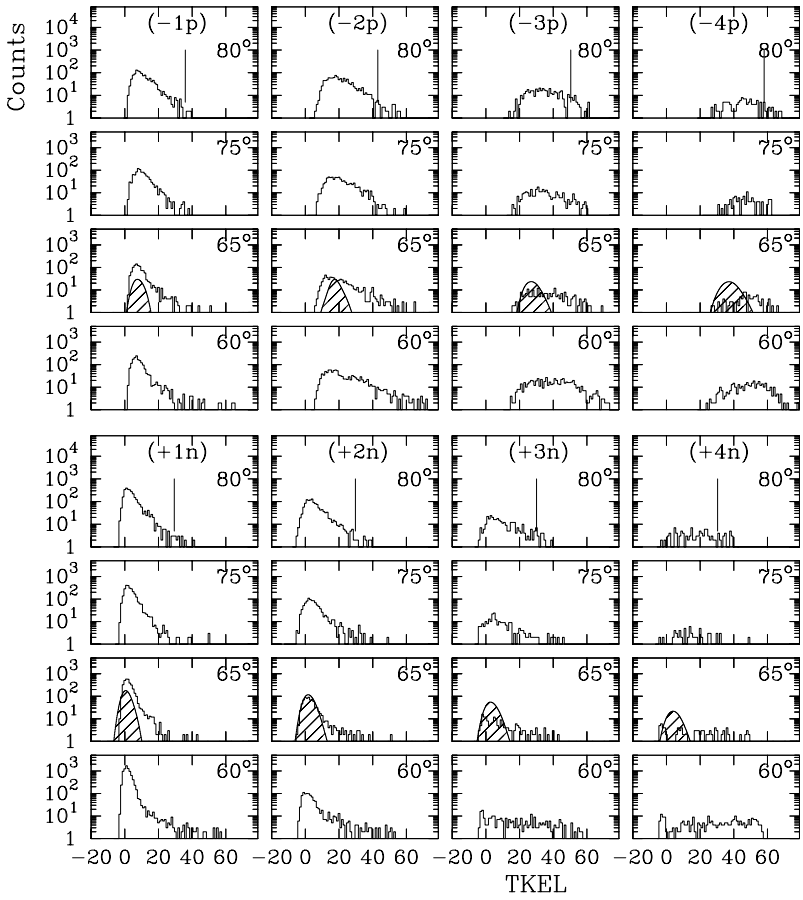

FIG. 5. Experimental (histogram) and theoretical (shaded areas) total kinetic energy loss distributions for the pure neutron pickup and proton stripping channels at $\theta_{\rm lab} = 60^\circ$, 65°, 75°, and 80° at $E_{\rm lab} = 249$ MeV.

which shows the spectra for several scattering angles). We tried to separate these two components for each scattering angle by making Q value cuts on the TKEL spectra. In all cases, at the maximum of the angular distributions the contribution of the fully relaxed events is less than 5%, whereas moving to forward or backward direction this contribution rises, for some channels, up to $\simeq 50\%$. Thus, we may conclude that in the grazing region, deep-inelastic processes do not significantly affect the total quasielastic cross section.

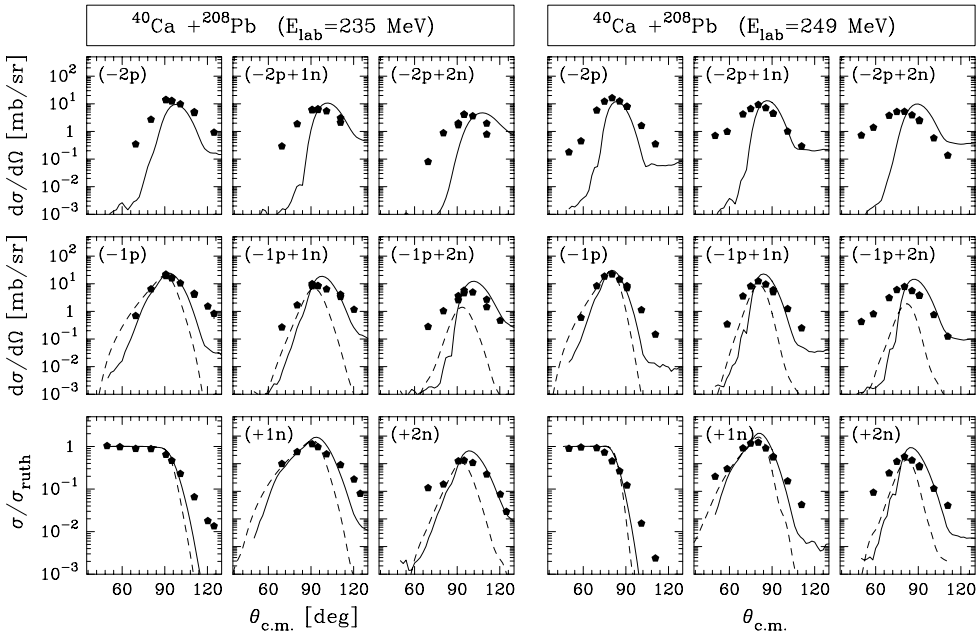

FIG. 6. Experimental (dots) and theoretical (lines) angular distributions of dominant transfer channels measured at $E_{\rm lab} = 235$ (left) and 249 (right) MeV and integrated over all detected energies. The full and dashed lines are results of CWKB and GRAZING calculations, respectively.

III. CALCULATIONS AND COMPARISON WITH THE DATA

The data are analyzed by using the semiclassical models GRAZING [7–9] and CWKB [6,13]. The treatment of the transfer degrees of freedom is, in both models, based on the assumption that in a heavy-ion collision the exchange of a nucleon may proceed via many open channels that are all quite weak, so that they may be treated as independent modes.

The semiclassical model GRAZING treats surface degrees of freedom and particle transfer on the same footing, the exchange of many nucleons proceeds via a multistep mechanism of single nucleons (both, protons and neutrons, via stripping, and pickup processes). The trajectory is calculated by solving the system of classical equations for the variables of relative motion and the deformation parameters for the surface modes. The model includes the low-lying 2^+ and 3^- states and the corresponding giant resonances.

The CWKB model uses the WKB approximation [6] for the radial wave functions and for the calculation of the first-order transfer amplitudes. The empirical potential of Ref. [14] is used as the real part, and the microscopically calculated [15,16] as the imaginary part of the optical potential. The multinucleon transfer channels were estimated from the multistep mechanism as in GRAZING and by explicitly including pair transfer modes. Here we take the opportunity to summarize the different steps taken to calculate the cross sections in the CWKB model, whereas for GRAZING we refer to the mentioned references.

The inclusive cross section for the one-nucleon transfer channel is written as a sum over all possible single-particle levels of projectile and target:

$$\left[\frac{d\sigma}{d\Omega}\right]_{\rm tr} = \sum_{a_i a_f \lambda} \frac{\kappa_f}{\kappa_i} \left| \sum_{\ell\mu} \frac{2\ell+1}{2i\kappa} c^{\lambda\mu}_{a_f a_i}(\ell) T(\ell) P_\ell(\cos\theta) \right|^2, \quad (1)$$

where, for the partial wave ℓ, $c^{\lambda\mu}_{a_f a_i}(\ell)$ is the first-order semiclassical amplitude for the transition from the single-particle level $a_i \equiv (n_i, l_i, j_i)$ to the single-particle level a_f and where $T(\ell)$ is the T-matrix for elastic scattering. The semiclassical amplitude $c^{\lambda\mu}_{a_f a_i}(\ell)$, which in the time-dependent picture is written as follows:

$$c^{\lambda\mu}_{a_f a_i}(\ell) = \sqrt{\frac{1}{4\pi\hbar^2}} D^\lambda_{\mu 0}\left(0, \frac{\pi}{2}, 0\right) \int_{-\infty}^{+\infty} dt\, f^{a_f a_i}_\lambda(r(t)) \times e^{\frac{i}{\hbar}[(\Delta E - Q_{\rm opt} + \Delta)t - \hbar\mu\phi(t)]} \quad (2)$$

is here evaluated in the complex WKB approximation [6]. The single-particle form factor $f^{a_f a_i}_\lambda(r(t))$ is calculated by a folding procedure from the single-particle wave functions in projectile and target.

The above formalism may be generalized for the calculation of multinucleon transfer reactions by exploiting the fact that each individual transition is very small. The probability p_{fi} for n_{fi} (=0, 1) transitions of the type fi (i.e., $a_i \to a_f$) can be written as follows:

$$p_{fi}(n_{fi}, \ell) = \begin{cases} p_{fi}(\ell) & \text{for } n_{fi} = 1 \\ 1 - p_{fi}(\ell) & \text{for } n_{fi} = 0, \end{cases} \quad (3)$$

where, in good approximation,

$$p_{fi}(\ell) = \sum_{\lambda\mu} \left| c^{\lambda\mu}_{a_f a_i}(\ell) \right|^2. \quad (4)$$

In the independent particle description a given transition may be represented with an ensemble $\{n_{fi}\}$ of numbers n_{fi} (=0, 1) indicating whether the single-particle transition fi occurred in the transition. The probability for this transition is thus given by the following:

$$p(\{n_{fi}\}, \ell) = \prod_{fi} p_{fi}(n_{fi}, \ell). \quad (5)$$

For example, the probability for the transfer of ΔZ charges can be calculated via a Monte Carlo procedure where, for each ℓ, the family of sequences $\{n_{fi}\}$ leading to that particular value ΔZ is statistically sampled. Thus,

$$P(\Delta Z, \ell) = \sum_{{\rm all}\{n_{fi}\}} \delta\left(\Delta Z - \sum_{i,f} n_{fi}\delta z_{fi}\right) p(\{n_{fi}\}, \ell), \quad (6)$$

where δz_{fi} is the charge quantum pertinent to the transition $a_i \to a_f$. For proton stripping, $\delta z_{fi} = -1$, whereas for proton pickup $\delta z_{fi} = +1$. The corresponding angular distribution is constructed using the following:

$$\left[\frac{d\sigma}{d\Omega}\right]_{\Delta Z} = \frac{\kappa_f}{\kappa_i} \left| \sum_\ell \frac{2\ell+1}{2i\kappa} \sqrt{P(\Delta Z, \ell)} e^{i\phi(T(\ell))} P_\ell(\cos\theta) \right|^2, \quad (7)$$

where $\phi(T(\ell))$ is the phase of the T-matrix in Eq. (1). In a similar way one may construct the probabilities and the cross sections for all other relevant quantities, such as ΔM, $E_{\rm loss}$, E^*_a, ..., specifying the exit channel. Equation (5) describes the population of multiple-particle transfer channels like $+2n$, $-2p$, $+2n$-$1p$, ... via a succession of independent single-particle transition steps. As discussed above, a direct transfer of correlated pairs is expected to play an important role in defining the final yields. The probability for the transfer of a pair of nucleons may be estimated from Eq. (2) by using the form factor for the transfer of two nucleons that is here calculated from the macroscopic prescription of Ref. [17]. Here the pair transfer couplings are of the following form:

$$F_P(r) = \beta_P \frac{\partial V(r)}{\partial A} \simeq \left(\frac{\beta_P R}{3A}\right) \frac{\partial V(r)}{\partial r}, \quad (8)$$

where the pair-deformation parameter β_P gives a measure of the correlation strength. The contribution of a multipair transfer is easily included in the calculation by adding transitions with $\delta z_{fi} = \pm 2$ for a pair of protons and $\delta n_{fi} = \pm 2$ for a pair of neutrons, in Eq. (6).

The empirical potential of Ref. [14], determined from a best-fit analysis of several elastic scattering angular distributions, has been used for the real part of the optical potential in the calculations of all cross sections. The imaginary part has been calculated microscopically following Refs. [15,16] with the same transfer channels used here to calculate the redistribution of mass and charge between ^{40}Ca and ^{208}Pb nuclei. To have a good position of the maxima in the angular distributions for the $+1n$ and $-1p$ inclusive cross sections

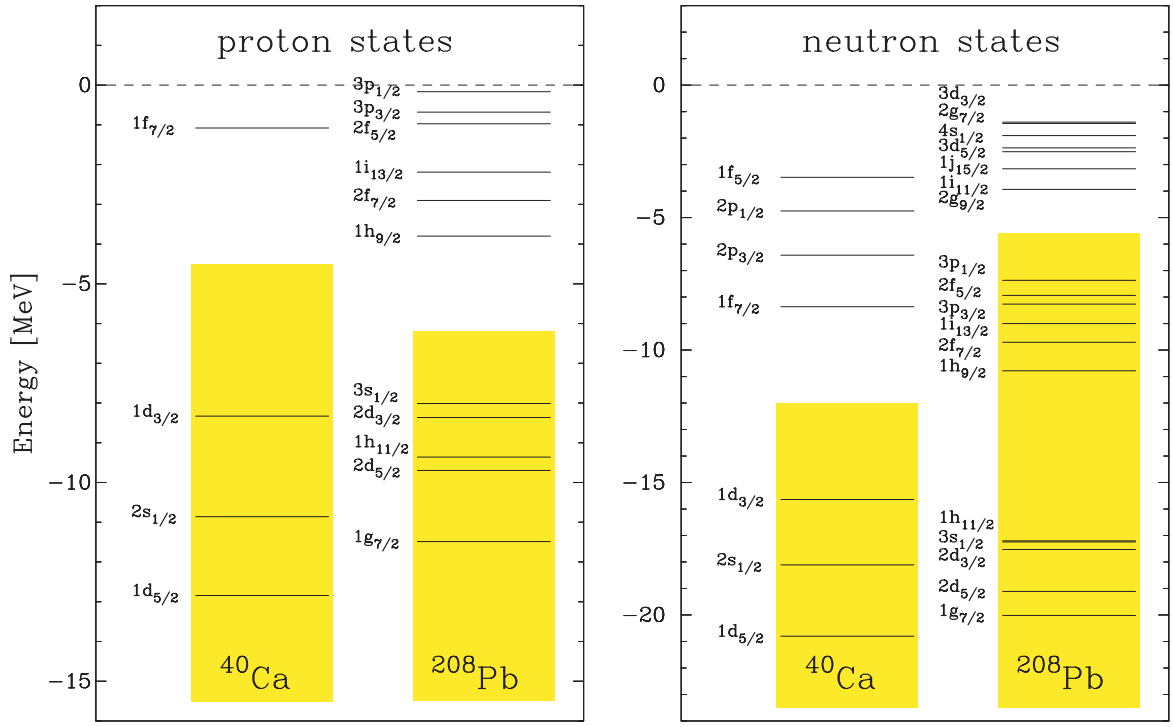

FIG. 7. (Color online) Single-particle levels for projectile and target used in the calculations. The gray areas indicate the occupied levels.

we had to increase the strength of the real potential while leaving the imaginary part unchanged. We choose to do that by increasing its radius by $\Delta R = 0.25$ fm. As discussed later, this potential also allows a very good description of the quasielastic angular distributions (see Fig. 8).

The full range of Q value explored by the reaction has been fulfilled by the inclusion of all transitions between the single-particle levels of projectile and target of a full shell below the Fermi surface and all single-particle levels above. For the present reaction, the single-particle states close to the Fermi surface are reasonably well known and we could use the available experimental information for most of them. They are reported in Fig. 7. In the construction of the form factors, the wave functions of the single-particle levels have been calculated by using the shell model potential of Ref. [18] for ^{40}Ca and the one of Ref. [19] for ^{208}Pb. The total inclusive cross sections for pure neutron and proton channels are shown in Fig. 2 with dashed lines. As seen, the theory describes the pure neutron pickup channels reasonably well but considerably underpredicts the pure two-proton stripping channels even if the one-proton stripping channel is described adequately.

To see if a better description of the data could be obtained, we have included pair-transfer modes for proton stripping and neutron pickup channels (the other two modes, neutron stripping and proton pickup, may be neglected for Q-value reasons). Only one pair-transfer mode for each channel ($-2p$ and $+2n$) located at the optimum Q value (-0.8 MeV for the $+2n$ and -17 MeV for the $-2p$ channel) was used, avoiding too many parameters. The strength of these form factors was kept the same for protons and neutrons and was fitted to the inclusive cross section of the $-2p$ channel thus obtaining a pair-deformation $\beta_p = 4.3$. The full-line histograms in Fig. 2 represent the results of such calculations for the two bombarding energies. The inclusion of the pair-transfer mode is essential for the description of the proton channels and does not alter the good results for the neutron channels.

The full isotopic distribution of the fragments in comparison with the data, for the bombarding energy of 249 MeV, is shown in Fig. 9. For this refined description, the yield redistribution generated by evaporation processes is taken into account. From the single-particle population of the final states we could extract the excitation energy and the angular momentum of the fragments. Then using the code PACE [20] we estimated the evaporation from the primary fragments. As mentioned in the experimental section, the inclusion of this process is essential for the description of the yields for the massive charge transfer channels that are shifted toward the lighter masses.

The angular distribution for some of the reaction channels is shown in Fig. 6 in comparison with the experimental data. The theory describes the angular distributions for most of the shown channels reasonably well but uderpredicts the forward angles for the transfer of many nucleons. This is a clear indication of the relevance of the surface degrees of freedom. Actually, it is the surface dynamics, governed by the low-lying modes, that allows the two ions to stay in close contact for longer times (i.e., to buildup the "neck" between the two colliding partners). As mentioned above, the program GRAZING treats the surface degrees of freedom and the particle transfer on the same footing. Angular distributions calculated with this model are also shown in the same figure with a dash-dotted line. Notice that GRAZING gives a better description of the

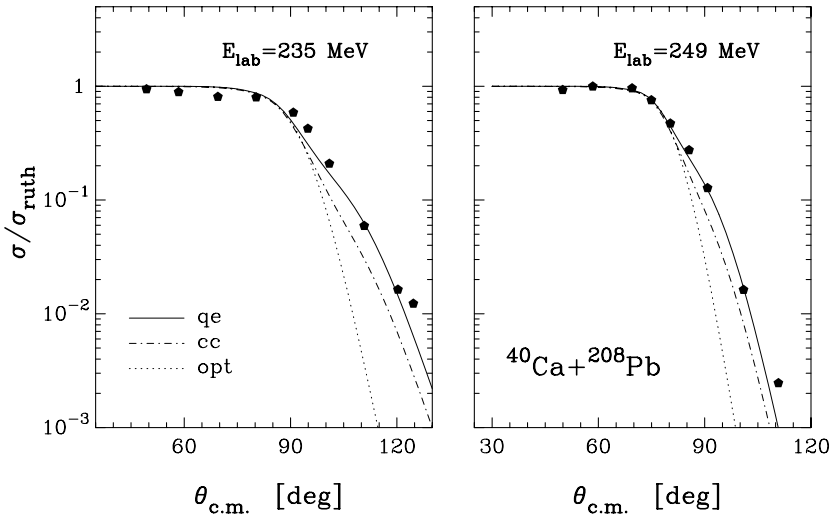

FIG. 8. Measured (points) and calculated (lines) quasielastic angular distributions. The calculations are obtained in the coupled-channel approach using the code PTOLEMY. The full lines represent quasielastic cross sections defined as the sum of the elastic (dash-dotted) and of all inelastic cross sections. With a dotted line we reported also the Optical Model elastic angular distributions.

angular distributions at forward angles. The same figure also shows the angular distributions (ratio to Rutherford) of the entrance-channel mass partition (that we call quasi-elastic) in comparison with the data. Although the theory gives a good prediction for the quarter point (the geometry and sizes of the potential are quite good), it misses the gentle falloff in the forward direction and has a too-sharp transition at backward angles. Again the treatment of the surface modes, strongly excited by the Coulomb interaction, is important.

The TKEL spectra at the lowest bombarding energy are shown, as shaded areas in Fig. 4, for the indicated channels and for a particular partial wave close to the grazing. The theoretical curves have been scaled by using only one common factor obtained by fitting the maxima of the $+1n$ channel. To show the evolution of the energy spectra as a function of the scattering angle, in Fig. 5 we represent the TKEL spectra for the pure protons and neutron channels at the higher bombarding energy (the theoretical spectra are reported only for the scattering angle of 65°). Because several partial waves contribute at a given angle, a better theoretical description of the spectra can be obtained by including deeper penetrating trajectories that gradually become important as more particles are transferred. Of course, higher energy contributions to the spectra could also have been obtained by using several components of the pair transfer modes, but we decided to keep the number of parameters at a minimum. The good description of the TKEL spectra for many of the channels indicates that the used shell-model space is adequate at these bombarding energies. The fact that for the massive transfer the tail at higher energy is missing is a further indication that in these reactions it is essential to have a good description of the dynamics of the two nuclear surfaces.

Previously we mentioned that the potential of Ref. [14] had to be made more attractive. To check this and, at the same time, to check the importance of the surface modes, we performed coupled-channel calculations with the code PTOLEMY [21] for the quasielastic angular distribution. We explicitly included the coupling to the 2^+ and 3^- states in ^{40}Ca and ^{208}Pb with the known B(Eλ). An absorptive potential was used to describe the depopulation of the entrance channels because of the transfer channels that could not be explicitly included into the calculation. These were calculated microscopically using the model of Refs. [15,16]. Figure 8 displays the quasielastic angular distributions in comparison with the

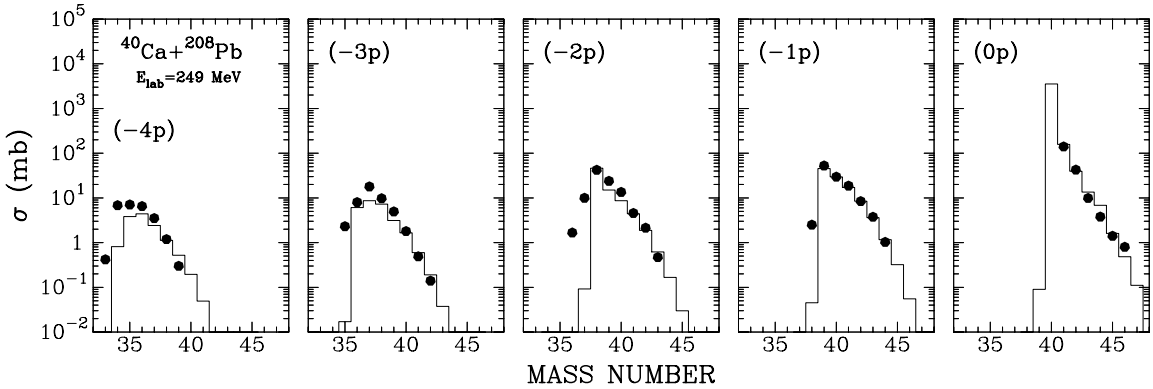

FIG. 9. Total angle and Q-value integrated cross sections for the transfer channels at $E_{lab} = 249$ MeV. Points and histograms are the experimental and theoretical values, respectively. The calculations shown include single and pair nucleon transfer modes and evaporation effects.

experimental data for the two bombarding energies. The quasielastic cross sections are defined here as the sum of the true elastic angular distribution (also reported in the figure) and of all the inelastic cross sections.

An overall good description of all multinucleon transfer data has been achieved by using standard parameters for the potentials and by employing models that incorporate the well-known properties of the two reactants, such as the single-particle states close to the Fermi surface and their surface collective modes. In particular, one observes that the pair-transfer mode gives an essential contribution to the proton transfer channels, whereas its contribution is almost negligible for the neutron channels. This proton and neutron asymmetric behavior, present in all reactions studied so far, should not lead us to think that pairing correlations are more important for protons than for neutrons. Nuclear structure calculations have, in fact, shown that the pairing interaction has the same strength for both of them. Because the one-neutron transfer cross section is almost one order of magnitude larger than the one-proton transfer, the contribution of a pair-transfer mode is masked, in the neutron sector, by the successive mechanism. As a last comment we note that the very short-range pairing interaction does not contribute directly to the transfer process but redistributes the strength around the pure particle-particle and hole-hole configurations of projectile and target. It is thus very difficult to deduce the effect of pairing correlation from inclusive cross sections (i.e., without the separation of the yields in the individual states).

IV. SUMMARY

In this article we have studied multinucleon transfer reactions in the ^{40}Ca+^{208}Pb collision at two incident energies close to the Coulomb barrier. The light reaction products have been detected with the time-of-flight spectrometer. The experimental observables, mass and charge yields, differential and total cross sections, and total kinetic energy loss distributions have been compared with those of semiclassical models. From this comparison we have learned that in addition to the well-known surface modes and the one-particle transfer channels, the transfer of correlated pairs of nucleons is important in description of the isotopic distribution of the reaction products. The importance of the evaporation has also been discussed. The theoretical models should evolve to incorporate all mentioned degrees of freedom consistently. In this way one should be able to describe the full body of quasielastic reactions and the transition to the more complex deep-inelastic reactions or to fusion.

[1] A. Bohr and B. Mottelson, *Nuclear Structure*, edited by W. A. Benjamin (Inc., New York, 1969), Vol. 1.
[2] W. von Oertzen, Z. Phys. A **342**, 177 (1992).
[3] K. E. Rehm, D. G. Kovar, W. Kutschera, M. Paul, G. Stephans, and J. L. Yntema, Phys. Rev. Lett. **51**, 1426 (1983).
[4] C. L. Jiang, K. E. Rehm, J. Gehring, B. Glagola, W. Kutschera, M. Rhein, and A. H. Wuosmaa, Phys. Lett. **B337**, 59 (1994).
[5] L. Corradi *et al*., Phys. Rev. C **66**, 024606 (2002).
[6] E. Vigezzi and A. Winther, Ann. Phys. (NY) **192**, 432 (1989).
[7] A. Winther, Nucl. Phys. **A572**, 191 (1994).
[8] A. Winther, Nucl. Phys. **A594**, 203 (1995).
[9] A. Winther, program GRAZING, http://www.to.infn.it/~nanni/grazing.
[10] S. Szilner *et al*., Eur. Phys. J. A **21**, 87 (2004).
[11] G. Montagnoli, F. Scarlassara, S. Beghini, A. Dal Bello, G. F. Segato, A. M. Stefanini, D. Ackermann, L. Corradi, J. H. He, and C. J. Lin, Nucl. Instr. and Meth. in Phys. Res. A **454**, 306 (2000).
[12] K. E. Rehm, A. M. van den Berg, J. J. Kolata, D. G. Kovar, W. Kutschera, G. Rosner, G. S. F. Stephans, and J. L. Yntema, Phys. Rev. C **37**, 2629 (1988).
[13] L. Corradi, A. M. Stefanini, D. Ackermann, S. Beghini, G. Montagnoli, C. Petrache, F. Scarlassara, C. H. Dasso, G. Pollarolo, and A. Winther, Phys. Rev. C **49**, 2875(R) (1994).
[14] R. A. Broglia and A. Winther, *Heavy Ion Reactions* (Addison-Wesley Pub. Co., Redwood City CA, 1991).
[15] R. A. Broglia, G. Pollarolo, and A. Winther, Nucl. Phys. **A361**, 307 (1981).
[16] G. Pollarolo, R. A. Broglia, and A. Winther, Nucl. Phys. **A406**, 369 (1983).
[17] C. H. Dasso and G. Pollarolo, Phys. Lett. **B155**, 223 (1985).
[18] Y. Eisen, H. T. Fortune, W. Henning, D. G. Kovar, S. Vigdor, and B. Zeidman, Phys. Rev. C **13**, 299 (1976).
[19] J. L. C. Ford, Jr., K. S. Toth, G. R. Satchler, D. C. Hensley, L. W. Owen, R. M. DeVries, R. M. Gaedke, P. J. Riley, and S. T. Thornton, Phys. Rev. C **10**, 1429 (1974).
[20] A. Gavron, Phys. Rev. C **21**, 230 (1980).
[21] M. H. Macfarlane and S. C. Pieper, PTOLEMY: A Program for Heavy-Ion Direct-Reaction Calculations, Report No. ANL-76-11, 1978 (unpublished).